Journal of Laser Applications

RESEARCH ARTICLE | OCTOBER 29 2024

Comparative analysis of laser power, pure titanium, and titanium alloy effects on dendrite growth and surface morphology of TiO_2-ceramic

Abid Ullah ; Karim Asami ; Kashif Azher ; Claus Emmelmann

J. Laser Appl. 36, 042061 (2024)
https://doi.org/10.2351/7.0001601

Journal of Laser Applications ARTICLE pubs.aip.org/lia/jla

Comparative analysis of laser power, pure titanium, and titanium alloy effects on dendrite growth and surface morphology of TiO_2-ceramic

Cite as: J. Laser Appl. 36, 042061 (2024); doi: 10.2351/7.0001601
Submitted: 1 July 2024 · Accepted: 16 October 2024 ·
Published Online: 29 October 2024

Abid Ullah,[1,2,a)] Karim Asami,[1] Kashif Azher,[3] and Claus Emmelmann[1]

AFFILIATIONS

[1]Institute of Laser and Systems Technology, Hamburg University of Technology, 21079 Hamburg, Germany
[2]Centre for Additive Manufacturing, School of Engineering, RMIT University, Melbourne, VIC 3000, Australia
[3]Department of Mechanical Engineering, King Fahd University of Petroleum & Minerals, 31261, Dhahran, Saudi Arabia

[a)]**Author to whom correspondence should be addressed; electronic mail:** abid.ullah@tuhh.de and abidmech95@gmail.com

ABSTRACT

Despite several challenges, including the inherent brittleness of ceramics, inadequate melting of the powder, and the formation of microstructural defects, laser powder bed fusion remains a promising method for ceramic fabrication. This research looks at the intricate relationship between laser power as a dominant factor in the energy density, the influence of pure titanium (Ti) and titanium alloy (Ti-6Al-4V) additives on the laser fabrication of TiO_2-based ceramics, and the resultant microstructural aspects, with a particular emphasis on dendritic growth and solidification defects. The research findings revealed that changing the laser energy density has a substantial influence on the dendrite growth and solidification rate of TiO_2 ceramic. However, in addition to optimizing the laser power, the addition of metal material additives also plays a significant role in regulating the melting state and controlling the part defects in ceramics. The findings support that the mixing of pure titanium showed a relatively favorable influence, enhancing the melting condition of TiO_2 and yielding a smooth surface with reduced defects. Conversely, the addition of a titanium alloy (Ti-6Al-4V) has a comparatively lower positive effect and led to the formation of substantial dendrites, solidification shrinkage, and significant fractures. The change in the scanning strategy from zigzag to island has no noticeable effect on the surface morphology and dendrite formation but contributes to controlling the spattering and crack propagation.

Key words: additive manufacturing, laser powder bed fusion, ceramics, surface morphology, dendrites, microstructures, titanium

I. INTRODUCTION

Laser powder bed fusion (LPBF), also known as selective laser melting (SLM), is an additive manufacturing (AM) technique that has gained significant attention in recent years due to its ability to fabricate complex geometries with high accuracy and precision.[1,2] Ceramics have the potential to execute the most stringent demands of today's industries. For example, advanced ceramic materials are resistant to abrasion and can endure high-temperature heat, making them ideal for a variety of applications. Ceramic materials are being utilized more often as insulators, conductors, and semiconductors, although they are constrained by temperature and pressure.[3,4] Ceramics processed through LPBF are highly important in the aerospace sector due to their high melting point, high strength, hardness, chemical stability, and low thermal and electrical conductivity.[5–8] However, various applications in the aerospace industry are also influenced by factors such as production cost, time, techniques, and the complexity of the components being manufactured. Traditional manufacturing techniques take longer and have many limitations, including high tool wear and shrinkage during the sintering process. For ceramic materials, compared to other materials, part defects are high, which has obstructed the applications of this technology.

The challenges associated with LPBF of ceramics include the difficulty in achieving uniform powder distribution and the risk of

thermal shock, asymmetric dendrites and grains growth, porosity, and cracking during the printing process.[9,10] However, ongoing research is discovering various approaches to overcome these challenges and improve the performance of LPBF printed ceramics. Liu *et al.*[11] studied crack defects in ceramic AM processes, emphasizing strategies to relieve them. Their work showed that the adjustment in parameters and material composition regulates molten pool flow, releasing thermal stress, refining grains, and toughening structures to resist crack initiation and growth. Huang *et al.*[12] investigated the solidification behavior and crack mechanisms in ceramics using a thermal model and the effects of changing laser parameters on cracking characteristics, demonstrating that controlled microstructure and parameters optimization are important in crack morphology and distribution. Chen *et al.*[13] investigated that particle size has a significant impact on the quality and performance of bulk samples, as well as fracture inhibition. Smaller particles were identified to be responsible for substantial volume shrinkage and decreased porosity, leading to improved mechanical performance. However, this study determined that surface microcracks were formed because of large volume shrinkage and were significantly healed by the sintering process, confirming that parts sintering is an efficient approach for the elimination of microcracks. Zheng *et al.*[14] studied the formation of cracks in alumina ceramics and classified the cracks into transverse and longitudinal cracks. Liu *et al.*[15] investigated the formation mechanisms and conducted the quantities analysis of pores in $Al2O_3$-ZrO_2 ceramic. Their research divided the pores of ceramic structures into four types: intercrystalline pore, interlayer pore, intralayer pore, and shrinkage pore. Zhang *et al.*[16] found that $ZrSiO_4$ enhances the flexural strength of silica-based ceramic cores by inhibiting crack propagation. However, these approaches have limitations, including poor surface quality, restricted part size and complexity, poor mechanical properties, and high costs. Further research is needed to identify the root causes of these defects and develop effective methods to improve the manufacturing process of ceramics.

Titanium dioxide (TiO_2)-based ceramics are valued for their exceptional characteristics and versatility in a wide range of applications ranging from advanced coatings to high-performance electronics.[17–20] Understanding the intricate interaction of processing variables and material behavior in TiO_2-ceramic composites is essential for reaching their full potential. In earlier research,[21] a study was conducted on the effect of specific LPBF process parameters (laser power and scanning speed) and material addition (only pure titanium) on the surface microstructure of pure titanium dioxide. However, there was still a need to further explore the material choices for addition in the form of Ti alloy, further increase into the pure Ti percent weight, and to investigate the variation in scanning strategy along with the optimized and increased laser power. In addition, the formation of dendritic structures, grain growth, and solidification defects requires further exploration in both the surface and cross sections of the specimens. In this study, we investigated the effect of Ti-6Al-4V alloy alongside pure Ti additives, allowing us to broadly compare the effects of these materials on the manufacturing process and microstructure of TiO_2 ceramic. Furthermore, we also adopted the island scanning strategy along with the zigzag strategy to provide a more detailed examination of microstructural changes and explore the influence of variation in scanning strategy on the fabrication of ceramics. Additionally, we carefully controlled and optimized the laser power within a specific range (80–170 W), which contributed to more stable processing conditions, consistent experimental results, and a reduction in surface defects. Our current study is distinguished by its in-depth analysis of dendrite formation and grain growth in the samples' surface and cross sections, offering a deeper understanding of surface microstructures, defects, and their correlation with different material additives, as well as laser power and scanning strategy as laser parameters.

II. EXPERIMENT

A. Materials and methods

The material powders used in this study are characterized as follows: TiO_2 powder with an average particle size of 3 μm (ranging from 1 to 5 μm), Ti powder with an average particle size of 1 μm (ranging from 0.5 to 2 μm), and Ti-6Al-4V alloy powder with an average particle size of 45 μm (ranging from 30 to 60 μm). The corresponding thermo-physical properties are TiO_2 with a melting point of approximately 1843 °C and a heat conductivity of 7.8–8.4 W/m K, Ti with a melting point of 1668 °C and a heat conductivity of 16.2–21.9 W/m K, and Ti-6Al-4V with a melting point range of 1600–1660 °C and a heat conductivity of 6.7–7.5 W/m K.

The purity of both TiO_2 and Ti powders was recorded as 99.89%. Experiments were conducted based on variations of laser power and material ratios. A slurry was prepared by mixing the powder with water at a powder-to-water weight ratio of 3:1. The purpose of the slurry was to facilitate the deposition of layers on the movable platform because it is difficult to maintain a layer of the powder due to the inherent properties of ceramics. The difficulty in maintaining a uniform powder layer is primarily due to the high brittleness, low flowability, and high cohesiveness of ceramic powders. Unlike metal powders, ceramic powders tend to form agglomerates and have poor flowability, making it challenging to spread them evenly across the build platform. Additionally, the brittle nature of ceramics can cause the particles to break during deposition, further complicating the formation of a consistent powder layer. In the next step, the water evaporated completely. The thickness of each layer was maintained at 50 μm, and each printed sample consisted of 25 layers. The size of each sample was 10×10 mm. The scanning speed was kept constant at 200 mm/s as in previous studies[21,22] considered this optimal for ceramics. For pure TiO_2 specimens, both island and zigzag scanning strategies were utilized, while only the zigzag scanning strategy was used for samples with metal additives. The hatch spacing was kept constant at 50 μm. Figure 1 shows the schematic diagram of the ceramic samples' fabrication process used in this study. The laser power parameters and material ratios are listed in Table I.

B. Experimental setup

The experiments were conducted in a self-built laboratory-scale laser powder bed fusion system containing a continuous fiber laser called the YLR-500 that has a wavelength of 1.06 μm and a maximal output of 500 W. Theoretically, the spot size of the laser beam was 70 μm The machine was also equipped with a 20 kW

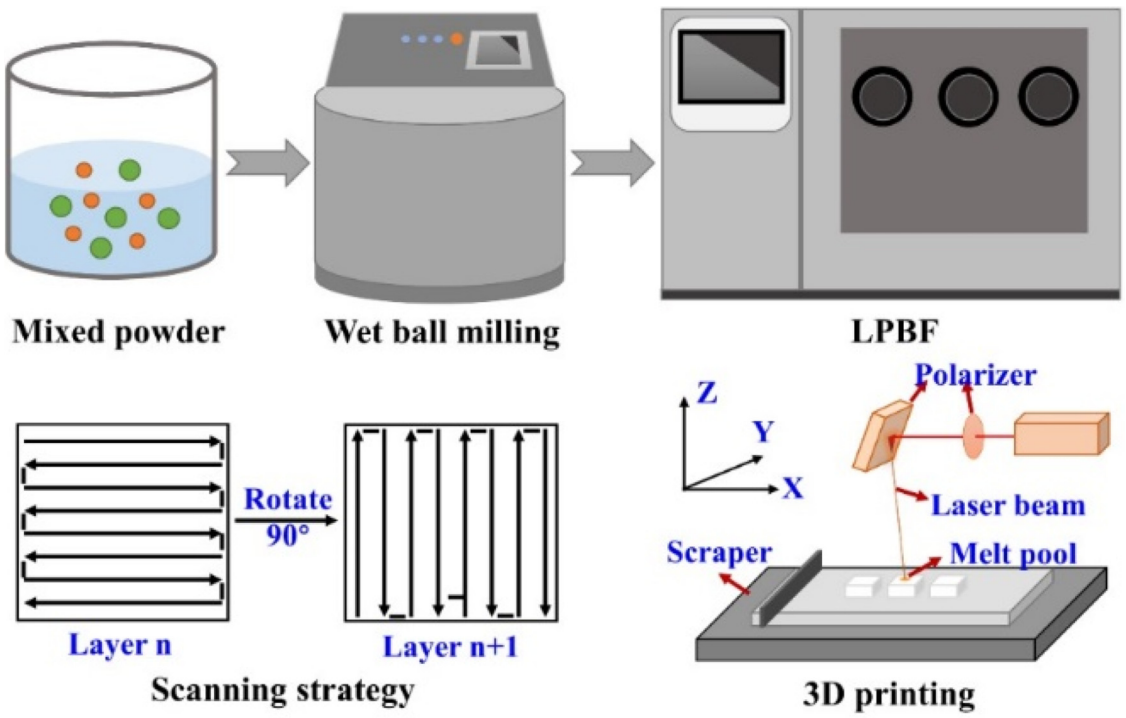

FIG. 1. Schematic diagram of the ceramic samples' fabrication process. From Zhang *et al.*, Smart Mater. Manuf. **2**, 100048 (2024). Copyright 2024 Author(s), licensed under a Creative Commons Attribution (CC BY) license.

induction heating system (Shanghai BamacIn), which was mainly used to preheat the substrate at a temperature of 110 °C to evaporate water from the deposited layer. As for the experimental conditions, these experiments were conducted in an open environment. For more details, please refer to the previous work where the experimental steps are fully described, as this study follows the same approach.[21–24]

TABLE I. Experimental parameters.

Material composition (wt. %)	Laser power (W)
TiO_2 = 100	80, 120, 170
TiO_2:Ti = 98:02	80, 120, 170
TiO_2:Ti = 95:05	80, 120, 170
TiO_2:Ti = 90:10	80, 120, 170
TiO_2:Ti = 85:15	80, 120, 170
TiO_2:Ti = 80:20	80, 120, 170
TiO_2:Ti = 75:25	80, 120, 170
TiO_2:Ti64 = 95:05	80, 120, 170
TiO_2:Ti64 = 90:10	80, 120, 170
TiO_2:Ti64 = 85:15	80, 120, 170
TiO_2:Ti64 = 80:20	80, 120, 170
TiO_2:Ti64 = 75:25	80, 120, 170

C. Measurements

A Leica EM ACE200 ion sputter coater was used for the samples' gold coating. To acquire high-resolution images and investigate the surface morphology and microstructure of the printed objects, a scanning electron microscope (SEM) (FEI Quanta 250F) was used. IMAGEJ software was used to analyze the SEM images. The parts' structure and formation of phases were determined using Bruker D8 x-ray diffraction (XRD). The XRD patterns were produced at room temperature using continuous mode Cu Kα radiation (=1.5418 Å) of 2θ = 10°–100° The XRD was run at 40 mA tube current, 40 kV target voltage, and 2°/min scan speed.

III. RESULTS AND DISCUSSION

Sections III A–III C discusses the experimental results on the effects of laser power, the addition of metal powders to TiO_2, and the influence of different scanning strategies.

A. Influence of laser power variations and the addition of Ti-6Al-4V and pure Ti on TiO_2

In this section, we analyze and compare the influence of Ti alloy and pure Ti on the melting behavior, manufacturability, and surface morphology of titanium dioxide fabricated by the LPBF process. In this study, "melting state" or melting condition" refers

to the ability of TiO_2 to absorb laser energy, reach its melting point, and form a homogenous melt pool with smoother and reduced surface defects. The pure titanium dioxide specimens were found to have several microstructural flaws, including microcracks, irregular dendrite and grain formation, porosity, and spattering effects. Similar defects have been widely investigated in previous studies of ceramic LPBF, where they were attributed to high-temperature gradients, inadequate melting, and rapid heating and cooling of the powder layers, as shown in Figs. 2(a) and 2(b). Our experimental results align with these prior findings.[21–23,25,26] The SEM images of the specimen reveal that asymmetrical grain and dendrite development serve as significant causes of crack formation. These phenomena are more common in specimens of pure titanium dioxide produced with lower laser energy input. Figures 2(a) and 2(b) show some fractures in the form of large cracks with a number of elongated grains and dendrite growths. The specimens also possess rough surfaces due to the spattering effect or partially melted materials, as identified in the LPBF of cuprous oxide,[22] possibly due to inadequate melting of the ceramic powder. Lowering the laser power decreases the energy input, leading to lower temperatures in the material and reduced temperature gradients, as described by Fourier's law of heat conduction. This, in turn, influences the solidification and cooling rates of the sintered or melted layers.[27] This implies that poor melting and rapid cooling of the powders causes some sort of interface instabilities and solidification defects, which turn into the formation of dendrites, as evident in Fig. 2(a). These dendrite structures are generally undesirable and considered the key causes of various microstructural defects including interdendritic fractures which are formed as a result of weak and complex boundary connections of the dendrite arms. During the poor melting of the powder, the mobility of powder particles along these dendrite boundaries may be limited, making it difficult for them to rearrange, distribute evenly, and eliminate defects. The defects found in Fig. 2(a) were reduced with an increase in the laser power from 80 to 120 W, which further supports the idea that high laser power contributes to the proper melting of the powders and reduces surface defects[21] as shown in Fig. 2(b). However, certain dendritic fragmentation along with surface roughness and microcracks still exist.

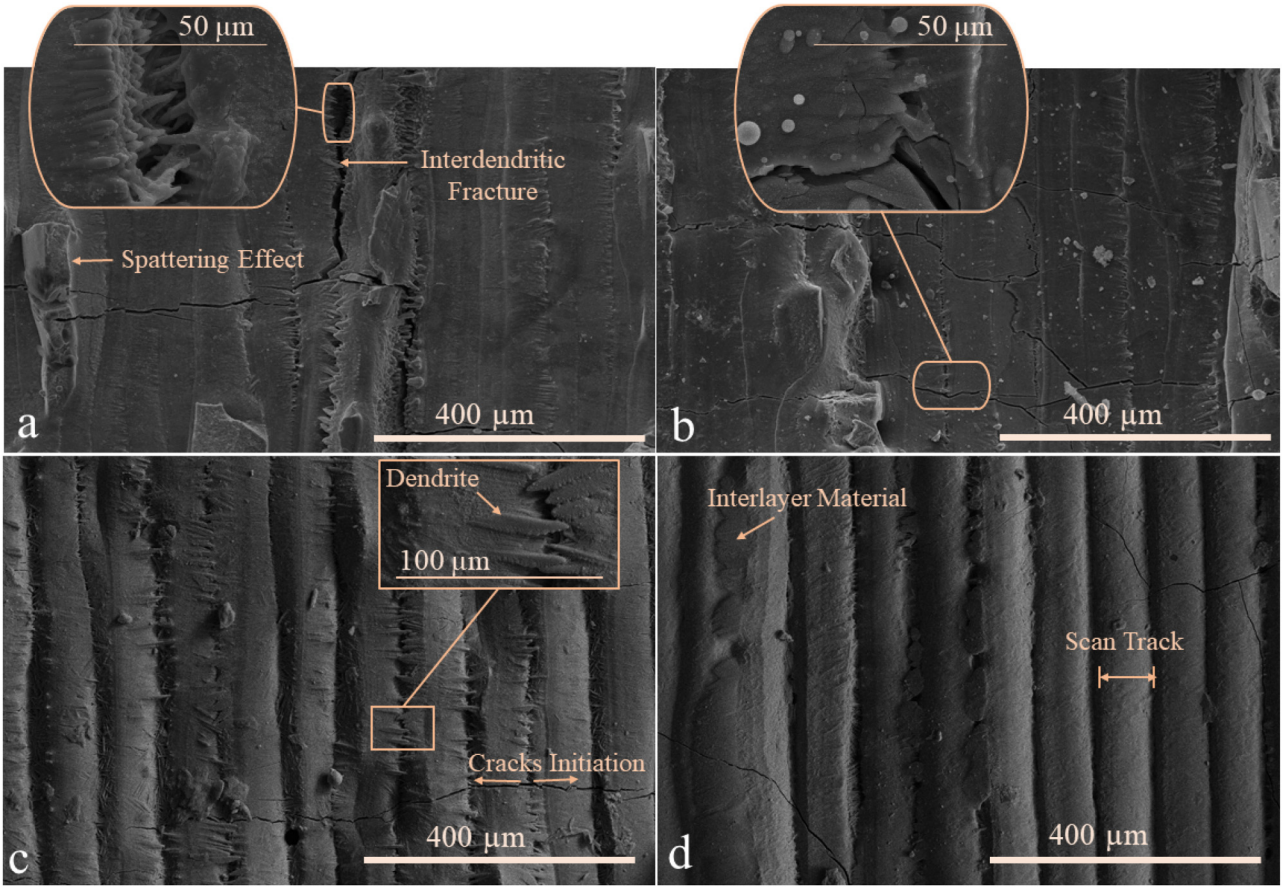

FIG. 2. (a) Pure TiO_2 at 90 W, (b) pure TiO_2 at 120 W, (c) TiO_2 90% with Ti64 10% at 90 W, and (d) TiO_2 90% with Ti64 10% at 120 W.

Considering the high melting point and poor heat conduction of ceramics, getting a high degree of densification becomes more difficult at lower energy input by the laser beam which can contribute to the higher level of microstructural defects in the fabricating specimens. In addition, the heat produced by the laser beam is distributed unevenly.[28] This uneven heat distribution is caused by factors such as the high concentration of energy at the center of the Gaussian beam, the poor heat conductivity of ceramics, and variations in heat absorption across different regions, which can result in thermal stresses and high-temperature gradients that contribute to creating several challenges including the above-mentioned defects in ceramics.[19,21] The addition of a titanium alloy (Ti-6Al-4V) reduced the surface defects including the formation of primary dendrite arms to some limit and enhanced the densification of the printing layers, as shown in Fig. 2(c). However, the surface morphology of the specimen shows that there are some deep lines or grooves between the adjacent scanning tracks while the scanning tracks tend to be raised (which seems like a protrusion effect) and sufficiently melted. It is also clearly observed that dendritic growth occurs along the boundaries of the scanning tracks. The dendritic arms form perpendicular to the laser's scanning direction and extend and intersect with the boundaries or edges of the neighbor scanning tracks. Microcracks propagating perpendicular to the scanning direction are also initiated from the origin of these dendrite structures. The cracks are caused by thermal stresses developed during the rapid heating and cooling cycles of the LPBF process.[14,25] As the laser moves along its path, the material in the near region rapidly heats and expands, while the surrounding material remains colder and more confined. When cooled, the heated material shrinks. This uneven thermal expansion and contraction generates stresses that are perpendicular to the scanning direction, resulting in cracking development since the material cannot withstand the tension. Figure 2(d) shows that the formation of dendrite arms was eliminated or largely reduced by increasing the laser power. Instead, there are some fused interlayer materials observed between the two adjacent scanning tracks, which apparently serve as a bridge to reinforce or further strengthen the tracks' boundaries. This phenomenon can result in smoother and more uniform surfaces between neighboring tracks. The melting paths are observed as raised and melted as a result of energy application, which are possibly caused by the immediate cooling and solidification of the molten powders after the laser passes. Although it is evident that there are still some microcracks and surface roughness, the results show that the addition of Ti-6Al-4V contributed to controlling the growth of asymmetric grains and dendrite formation, reducing the formation of large cracks, and ultimately leading to improved surface morphology. The possible reason behind this is that Ti-6Al-4V, with its comparatively lower melting range (1600–1660 °C) compared to titanium dioxide (~1843 °C), melts more easily and transfers the absorbed energy to the surrounding titanium dioxide particles, ultimately helping to improve the overall melting conditions of the deposited powder layer. The formation of primary dendrite arms along with other defects are largely reduced, which shows that Ti-6Al-4V served as a nucleation site for the crystallization of titanium dioxide during the solidification process. This also indicates that adding Ti-6Al-4V to TiO_2 ceramic stimulates the melting state of the powder and produces a uniform crystalline structure, both of which eventually prevent the formation of structural defects such as irregular dendrites in addition to surface defects like cracks and porosity. Previous studies show that lack of fusion during the LPBF process is a primary defect that leads to several other issues. Poor melting results in insufficient fusion, while improved and proper melting of the powder reduces these defects. By ensuring better melting, defects such as cracks, porosity, and irregular formations can be minimized.[29–31]

In the prior research, the influence of pure Ti was explored to some extent, which revealed some enhancements in the surface morphology of the printed parts.[21] Here, we further explore the impact of increased weight percent (2–30 wt. %) of pure Ti and variable laser power. The addition of a small weight (<5 wt. %) of Ti has the least influence on the LPBF of TiO_2 specimens. As revealed in Fig. 3(a), the specimens produced with a 2% weight of Ti have some defects, such as keyhole porosity, cracks, dendritic development, and spatters or defects caused by partly melted powder. However, compared to Fig. 2(a), there is a slight improvement in controlling the cracks and grain growth developments. This indicates that the printing of pure Titania ceramics exhibits significant microstructure and surface flaws due to its poor thermal conductivity, high heat resistance, and low laser energy absorptivity, as mentioned earlier. Figures 3(c) and 3(d) show that increasing the amount of pure Ti results in a reduction of surface defects, including cracks and pores. These changes indicate improved melting and fusion conditions, which are associated with the increased Ti content. The surface defects seen in Figs. 2(a) and 2(b) were almost entirely removed or substantially reduced, as seen in Fig. 3(c), by adding 10 wt. % Ti. However, there are some tree-shaped solidified surfaces observed in the specimens at higher magnification, which seems different from the dendrite shapes observed in Figs. 2(a)–2(c). The laser melts the powder along its path and produces localized regions of high heat. As these regions cool rapidly, they can lead to the formation of solidified structures, which are observed as dendrites. Dendrites are frequently observed during solidification processes, as also discussed by Refs. 32–34. These structures exhibit both branched and tree-like growth similar to the ones seen in these samples. However, in the case of this study, it appears that there is no clear association between this form of solidification effect and the defects formation, other than the micro surface roughness they caused. In this case, it is critical to closely monitor the process and further comprehend the complexity of the laser-material interaction.

The influence of increasing weight percent of Ti-6Al-4V and pure Ti was further investigated along with increasing laser power to 120 W. Figures 4(a) and 3(c) show that the growth of irregular dendrites structure and formation of defects were largely reduced by increasing the wt. % of Ti64 and pure Ti to 20%, respectively. Compared to Fig. 2(c), the formation of solidification dendrites on the edges of scanning tracks was prevented, which helped to control other defects and produced a significantly improved surface morphology, though some minor defects remained, as shown in Fig. 4(a). The melting paths are still observed as raised along with deep and narrow grooves or lines on the sides, which are possibly caused by the solidification and large particle sizes of the powder. However, increasing the laser power to a certain limit also plays an important role in improving the melting of the powders and

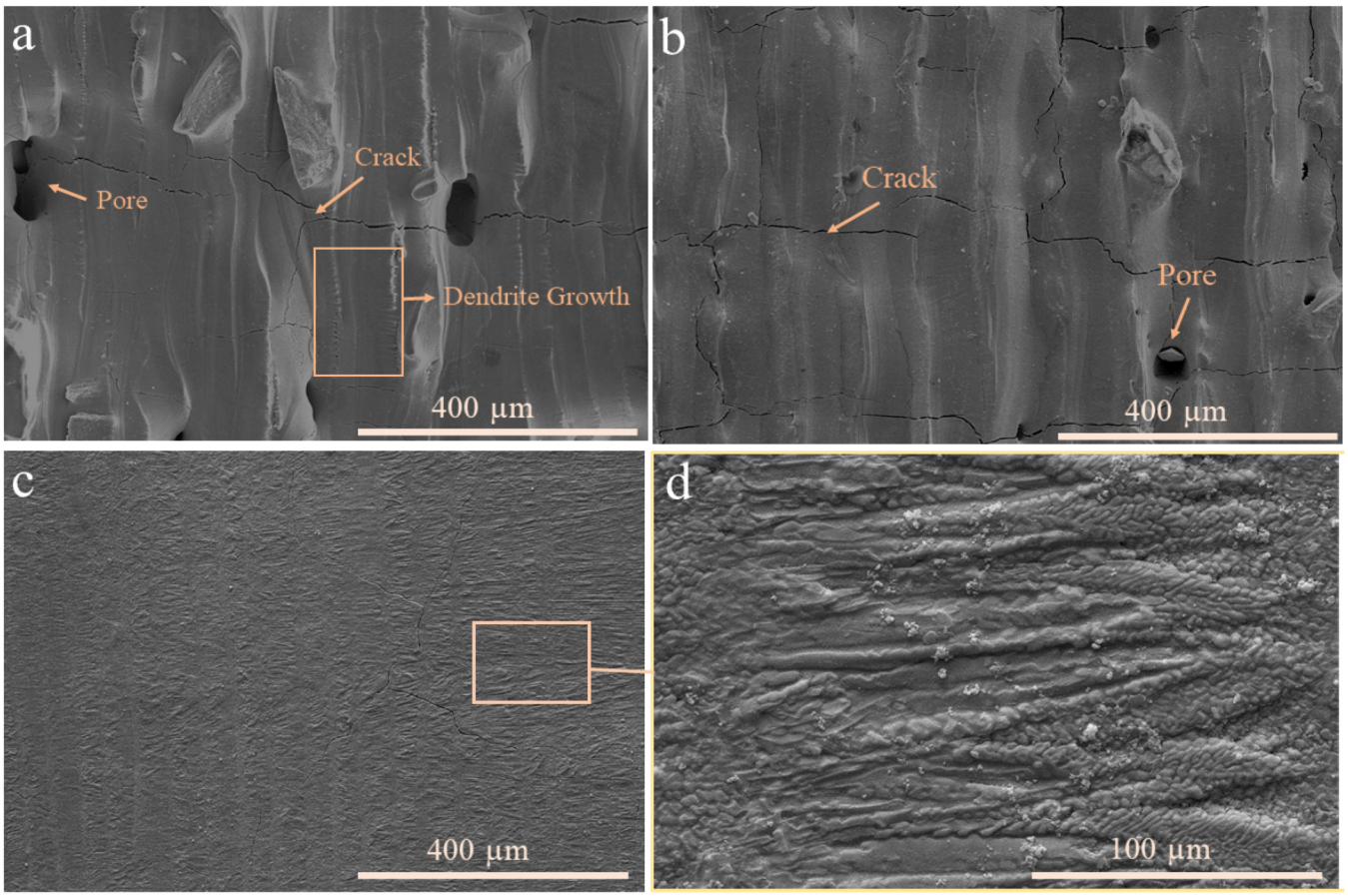

FIG. 3. (a) TiO_2 98% with 2% Ti at 80 W, (b) TiO_2 95% with Ti 5% at 80 W, (c) and (d) TiO_2 90% with Ti 10% at 80 W.

controlling defects, as reported in previous research.[14,21,25] In this study, 120 W was determined to be sufficient for melting the Ti-based powder at a scan speed of 200 mm/s. Similarly, with an increase in the amount of pure Ti to 20 wt. %, there were dramatic improvements in the overall melting condition of the powder and controlling the surface defects, as shown in Fig. 4(c). The effect of a further increase in Ti-6Al-4V and pure Ti up to 25 wt. % was tested at a higher laser power of 120 W. The formation of large and irregular grains' development was prevented but some unusually large fractures are observed at higher wt. % of Ti-6Al-4V, as shown in Fig. 4(b). Similarly, large crack fractures are seen in the samples fabricated with 25 wt. % of pure Ti. Further increasing the metal powder content poses a risk due to the high thermal conductivity of the metal, which can lead to rapid heat transfer, chances of overheating, and flammable oxidation of the powder in open air. At the same time, the thermal energy absorbed by the powder was transferred to the substrate (made of pure alumina), resulting in thermal expansion and cracks in the alumina substrate, which could be a major cause of the massive fractures in the built layers. A proper setup is required to develop for the experiments with a high %age weight of Ti (≥25%) that would involve using an inert gas environment with controlled oxidation to convert Ti into TiO_2, optimized laser parameters to prevent overheating while ensuring sufficient energy absorption, and temperature control of the substrate to manage thermal expansion and promote uniform oxidation and melting.

Compared to the first set of experiments with lower wt. % of Ti-6Al-4V and pure Ti addition, the apparent burning of the powder during the laser materials interaction was more intense, indicating that the addition of a higher amount of pure Ti or alloy contributed to more effective melting of the powder. As described in the previous discussion, the main possible reasons for sufficient melting of the powder and controlling of defects are that Ti and Ti-6Al-4V have lower melting points, high laser absorptivity, and relatively high thermal conductivity, which facilitate the melting process of TiO_2 ceramic. The sufficient melting of the powder is the key to controlling defects in the ceramic LPBF process, which was nearly achieved by the addition of the pure metal materials to TiO_2.

The cross sections of the specimens produced with pure TiO_2, 15% of Ti64, and 15% of pure Ti are presented in Fig. 5. The pure

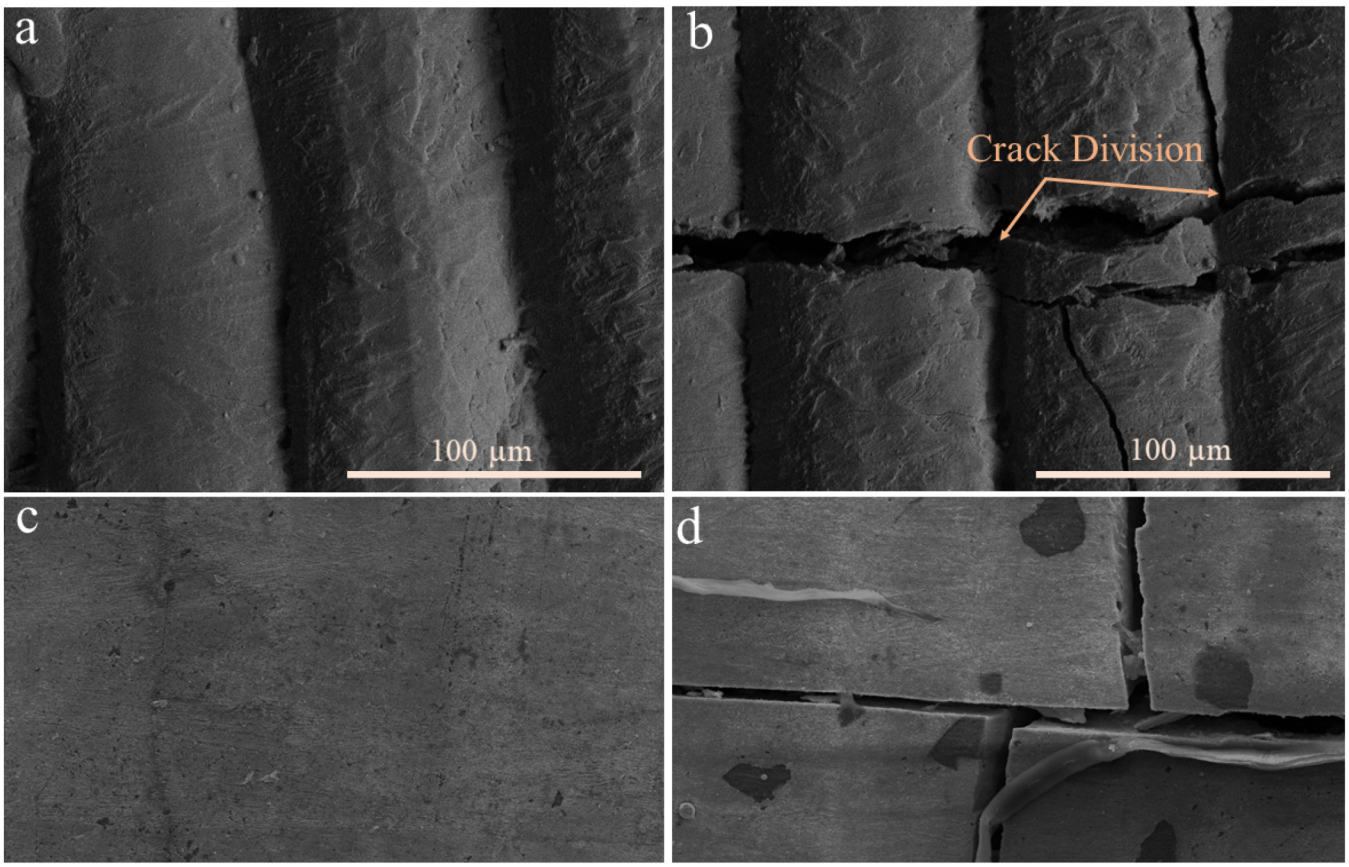

FIG. 4. SEM images of the specimens produced at 120 W and scanning speed 200 mm/s (a) TiO_2 80% with Ti64 20%, (b) TiO_2 75% with Ti64 25%, (c) TiO_2 80% with Ti 20%, and (d) TiO_2 75% with Ti 25%.

TiO_2 specimens display two primary types of surfaces, which we refer to as zones 1 and 2, as shown in Fig. 5(a). Zone 1 is largely dispersed in the upper portion of the cross section, with small dendritic structures which can be also called a dendritic zone, while zone 2 seems to be melted adequately. Some large dendritic tree formations can be seen on the boundary between the two zones. Zone 1 does not appear to have any dendritic structures and seems to have adequately melted. It is possible that the temperature in this zone was high enough for a sufficient amount of time to completely melt the powder and remove any pre-existing dendritic structures. This region's molten pool may be cooled sufficiently slowly to prevent dendrite growth, producing a more uniform microstructure. The combined actions of the heated substrate, the previously solidified layers below, and the thorough deposition of the new layer serve as the reason for this homogeneous cooling. The heated substrate and previously solidified layers act as heat reservoirs, gradually releasing heat during the cooling process. This helps maintain a stable thermal environment, encouraging a more controlled cooling and solidification process, which prevents rapid temperature fluctuations and reduces the likelihood of defects such as uneven dendritic growth. The small dendritic structures in zone 1 indicate that the temperature here was different from the melted zone. These dendrites likely formed as a result of less stable thermal conditions and faster cooling rates.[35,36] The boundary between the melted zone and the dendritic zone contains comparatively large dendritic tree formations. The tree-shaped dendrites were able to form in the border zone possibly due to the intermediate cooling rates. This may be the result of dynamics of partial melting and solidification impacted by the closeness to both dendritic and completely melted areas. The overall scenario indicates that there is no homogeneous heat transformation in the laser manufacturing of pure ceramics, leading to significant abnormalities, including the formation of dendritic structures and grain growth. By mixing in some Ti-6Al-4V and pure Ti, the solidification irregularities in the pure TiO_2 ceramic were evacuated, as shown in Figs. 5(b) and 5(c), respectively. However, the sample containing 15% pure Ti does not appear to have any porosity or dendritic structures, but the sample containing 15% Ti-6Al-4V does exhibit some porosity. This again confirms that adding an amount of pure Ti improves heat dissipation due to its high

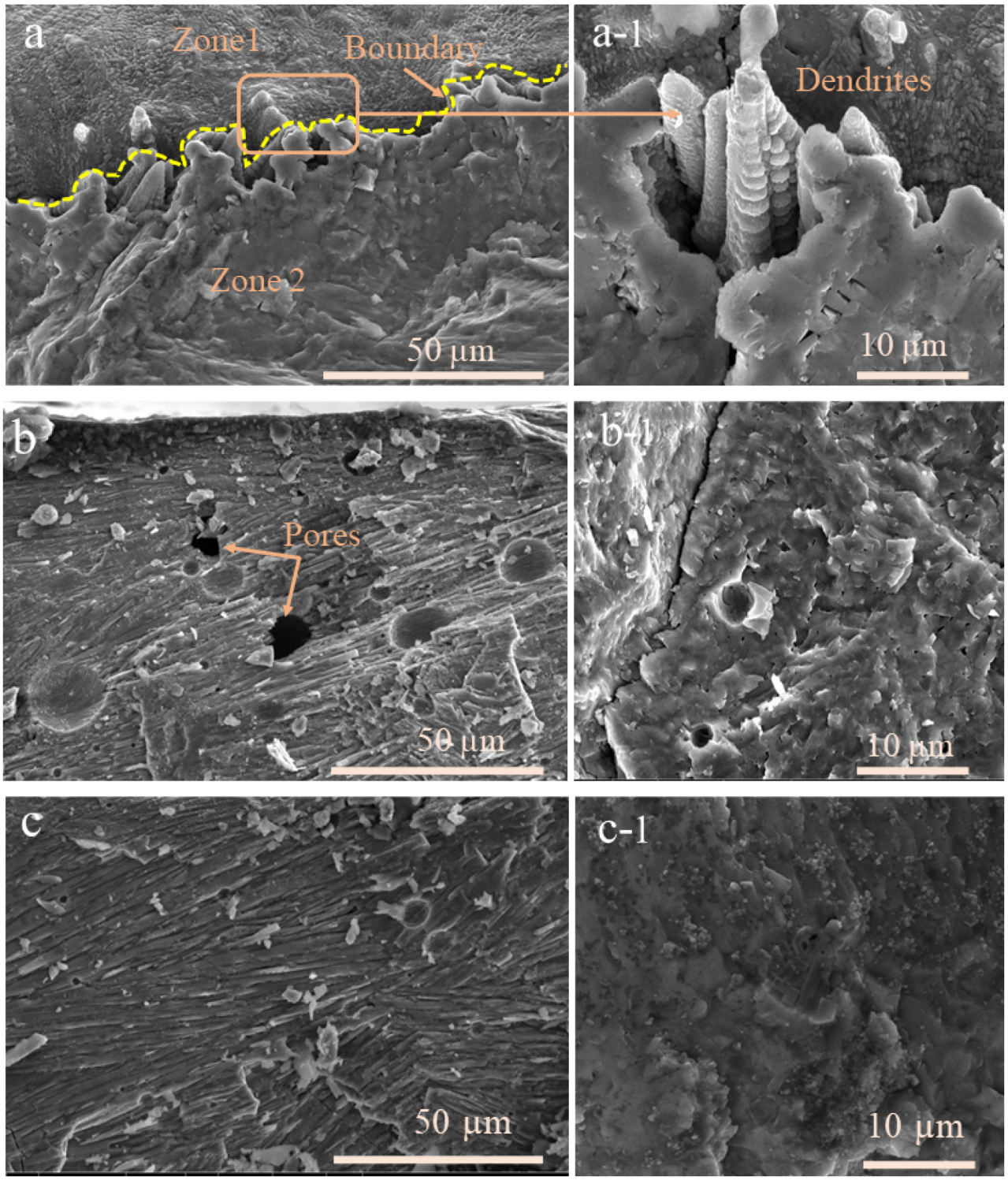

FIG. 5. Cross section of the specimens produced with (a) and (a-1) pure TiO_2, (b) and (b-1) 15% of Ti64, and (c) and (c-1) 15% of pure Ti at laser power 120 W and scanning speed 200 mm/s.

thermal conductivity (~21.6 W m^{-1}) and causes a more even-balanced cooling process that leaves the microstructure homogenous and clear of porosity and dendritic formations. The simpler chemistry of pure titanium encourages small grain structures and stable solidification.[37,38] On the other hand, adding Ti-6Al-4V introduced some porosity as shown in Fig. 5(b), which might be linked to its complex alloy composition which includes aluminum and vanadium. The presence of multiple alloying elements can lead to nonuniform solidification kinetics.[27,28] This nonuniform solidification may cause localized stresses due to the varying thermal properties of the alloying elements, potentially leading to the formation of porosity. Experiments were also conducted with more than 120 W laser power levels, which indicated substantial abnormalities and layer distortions due to high energy input. Raising the laser power to 170 W, certain tracks evaporated and warped, making it unfeasible to complete the desired layers.

B. Effect of scanning strategy

Several studies have been conducted on the effect of scan strategies on the surface morphology and microstructure of printing parts and have shown their influence, particularly in metal LPBF research. In this study, two scanning strategies, zigzag and island scanning strategies, were considered to test their effect on the microstructure, surface morphology, overall melting behavior, and part quality of the TiO_2-based ceramic. The zigzag scanning strategy involves a continuous back-and-forth motion across a $10 \times 10\ mm^2$ surface, while the island scanning strategy divides the same surface into 16 islands, arranged in four rows and four columns, with each island scanned individually in a specific sequence, similarly adopted in Ref. 14. The apparent surface morphologies of the samples show that there is no significant effect of the scanning strategy compared to the laser energy density and the addition of metallic materials. However, a minimal effect on crack initiation and suppression and porosity was observed, which was also noticed in the LPBF of alumina ceramics. The overall results based on the SEM of the surface morphology of the pure TiO_2 specimens show that the zigzag scanning strategy produced cracks in both vertical and horizontal directions, which are mainly initiated from the point of cracks bifurcation, leading to intricate crack network as shown in Fig. 6(a). On the other hand, the samples produced with the island scanning strategy show cracks in only the horizontal direction, which were named transverse cracks by Zhang *et al.*[39] In addition, the sample produced with zigzag scanning shows plenty of spatters, which are likely composed of unmelted or partially melted powders while the samples produced with Island scanning show some cavities identical to keyholes, as shown in Fig. 6(b). These voids suggest localized melting issues that lead to incomplete fusion and porosity. The overlap of melting tracks is also observed, which may contribute to the prevention of bifurcation and the controlling of cracks in vertical directions. This overlap might be caused by the maximum internal temperature, which is comparatively higher for island scanning.[39,40]

Overall, the effect of the scanning strategy is not very significant. This could be due to the specific strategies used or the experimental conditions applied. There is a possibility that these conditions may not have been ideal for fully capturing the impact of the scanning strategy; therefore, a future investigation to explore this area in more depth is recommended, especially focusing on its influence on the microstructure and surface morphology in ceramics.

C. X-ray diffraction analysis

XRD study of pure TiO_2, TiO_2-Ti64, and TiO_2-Ti specimens produced at moderate laser power (120 W for TiO_2) revealed that the addition of metals had no evident effect on the sample's crystalline structure. However, as demonstrated in Fig. 7, the samples produced with the addition of pure Ti and Ti alloy have a higher peak intensity and are more refined. The stability and increase in peak intensity may indicate the refined crystalline structure with a small grain size. In addition, there is no peak detected for pure Ti or Ti64. This also supports the previous findings where more refined microstructures with smaller grain sizes were obtained, and the metal powder was completely converted to oxide ceramic by oxidation.[21]

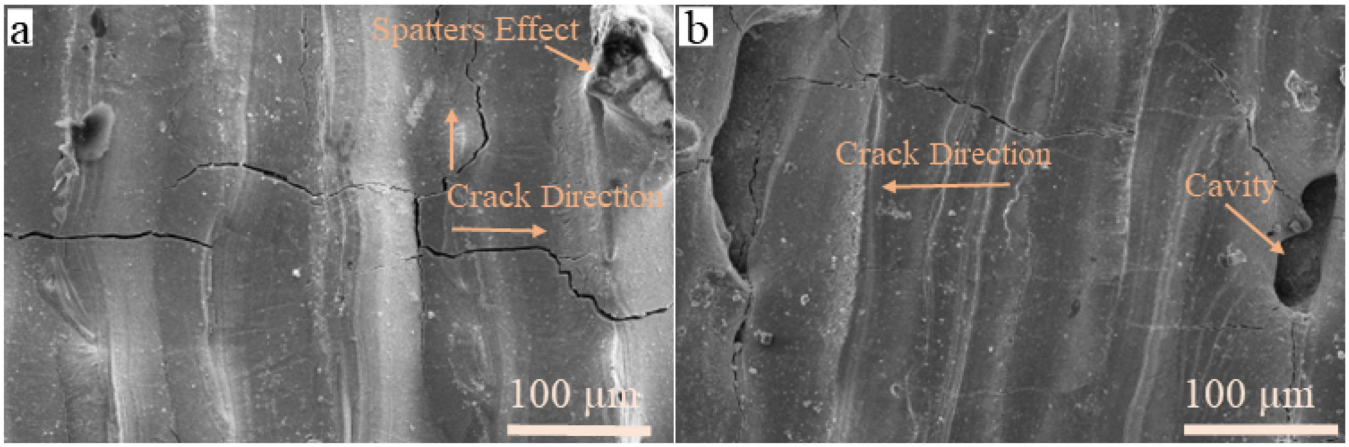

FIG. 6. Surface morphology of pure TiO_2 at laser power 90 W with (a) zigzag scanning and (b) island scanning strategy.

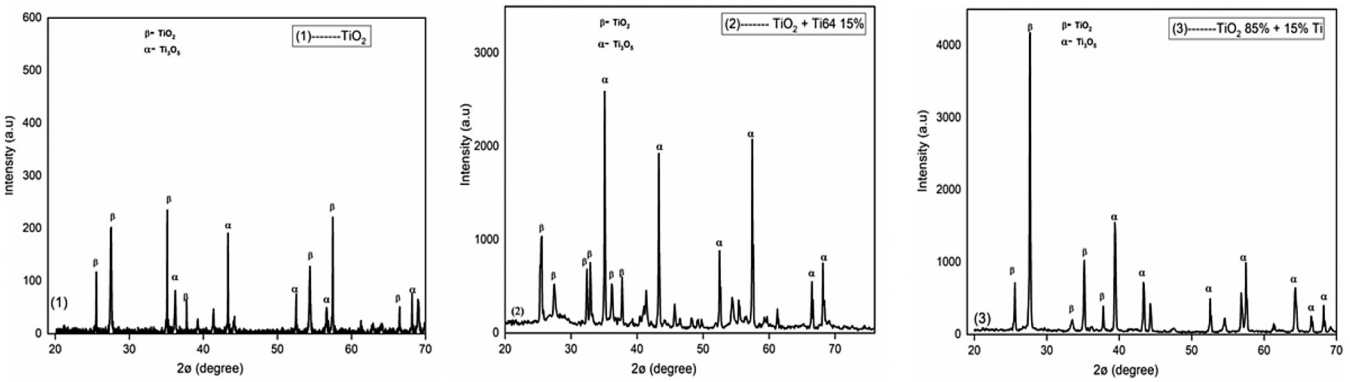

FIG. 7. XRD analysis of pure TiO_2, TiO_2-Ti64, and TiO_2-Ti.

IV. CONCLUSION

The printing of pure ceramics using direct laser melting presents significant challenges. The pure titanium dioxide (TiO_2) specimens exhibited numerous microstructural flaws, including microcracks, irregular dendrite and grain formation, porosity, and spattering effects. This research focused on enhancing the manufacturability of TiO_2-based ceramics and reducing part defects including irregular dendrite growth through the addition of Ti-6Al-4V and pure Ti powders using the LPBF process. The following are the main conclusion points:

1. The addition of Ti and Ti-6Al-4V powders improves the surface morphology and microstructure of the final specimens by enhancing melting behavior, resulting in more uniform melting and solidification. A comparative analysis was conducted to understand the distinct effects of Ti-6Al-4V versus pure Ti. The experimental findings revealed that adding a small amount of pure Ti improves the melting process and results in a more evenly balanced cooling process, leading to a smooth surface, free of porosity, and dendritic formations. Future studies could include a detailed investigation of the absorptivity behavior to further support this conclusion.
2. The surface morphology of the samples with pure Ti additions was cleaner, with fewer large grains, porosity, and dendrites compared to those with pure TiO_2 and Ti-6Al-4V. Additionally, the impact of the scanning strategy was investigated. It was found that the scanning strategy had minimal effect, except that the island scan produced only horizontal cracks with some cavities, while the zigzag scanning produced both horizontal and vertical cracks along with some spatters composed of unmelted or partially melted powder. However, further investigation is required to explore in-depth the influence of scan strategy on the microstructure and surface morphology of ceramics using the LPBF process.
3. The XRD analysis indicated that a more refined microstructure was achieved by adding metal powders, with the effect of pure Ti being more desirable compared to Ti-6Al-4V alloy.

ACKNOWLEDGMENTS

The first author works under the REDI Program, which has received funding from the European Union's Horizon 2020 Research and Innovation Program under the Marie Skłodowska-Curie Grant Agreement No. 101034328. This paper reflects only the author's view and the Research Executive Agency, and the European Commission are not responsible for any use that may be made of the information it contains. We also acknowledge Liu Tinting from Nanjing University of Science and Technology, China for her supervision and support of the experimental work.

AUTHOR DECLARATIONS

Conflict of Interest

The authors have no conflicts to disclose.

Author Contributions

Abid Ullah: Conceptualization (lead); Data curation (lead); Formal analysis (lead); Funding acquisition (equal); Investigation (lead); Methodology (equal); Project administration (equal); Resources (equal); Visualization (equal); Writing – original draft (lead); Writing – review & editing (equal). **Karim Asami:** Funding acquisition (supporting); Investigation (supporting); Project administration (equal); Resources (equal); Software (equal); Supervision (equal); Validation (equal); Writing – review & editing (equal). **Kashif Azher:** Conceptualization (supporting); Funding acquisition (supporting); Investigation (equal); Methodology (supporting); Writing – review & editing (equal). **Claus Emmelmann:** Project administration (equal); Resources (equal); Supervision (equal); Validation (equal); Writing – review & editing (equal).

REFERENCES

[1]S. Chowdhury, N. Yadaiah, C. Prakash, S. Ramakrishna, S. Dixit, L. R. Gupta, and D. Buddhi, "Laser powder bed fusion: A state-of-the-art review of the technology, materials, properties & defects, and numerical modelling," J. Mater. Res. Technol. **20**, 2109–2172 (2022).

[2]I. Adamov, G. Stanojević, S. M. Pavlović, D. Medarević, B. Ivković, D. Kočović, and S. Ibrić, "Powder bed fusion–laser beam (PBF-LB) three-dimensional (3D) printing: Influence of laser hatching distance on the properties of zolpidem tartrate tablets," Int. J. Pharm. **657**, 124161 (2024).
[3]Y. Lakhdar, C. Tuck, J. Binner, A. Terry, and R. Goodridge, "Additive manufacturing of advanced ceramic materials," Prog. Mater. Sci. **116**, 100736 (2021).
[4]T. Ayode Otitoju, P. Ugochukwu Okoye, G. Chen, Y. Li, M. Onyeka Okoye, and S. Li, "Advanced ceramic components: Materials, fabrication, and applications," J. Ind. Eng. Chem. **85**, 34–65 (2020).
[5]P. M. Gopal, V. Kavimani, K. Gupta, and D. Marinkovic, "Laser-based manufacturing of ceramics: A review," Micromachines (Basel) **14**, 1564 (2023).
[6]M. Dadkhah, J.-M. Tulliani, A. Saboori, and L. Iuliano, "Additive manufacturing of ceramics: Advances, challenges, and outlook," J. Eur. Ceram. Soc. **43**, 6635–6664 (2023).
[7]S. Bose, E. K. Akdogan, V. K. Balla, S. Ciliveri, P. Colombo, G. Franchin, N. Ku, P. Kushram, F. Niu, J. Pelz, A. Rosenberger, A. Safari, Z. Seeley, R. W. Trice, L. Vargas-Gonzalez, J. P. Youngblood, and A. Bandyopadhyay, "3D printing of ceramics: Advantages, challenges, applications, and perspectives," J. Am. Ceram. Soc. **107**, 7879–7920 (2024).
[8]J. F. Valera-Jiménez, J. R. Marín-Rueda, J. C. Pérez-Flores, M. Castro-García, and J. Canales-Vázquez, "Additive manufacturing of functional ceramics," in *3D Printing for Energy Applications* (Wiley, Hoboken, 2021), pp. 33–67.
[9]Q. Diao, Y. Zeng, and J. Chen, "The applications and latest progress of ceramic 3D printing," Addit. Manuf. Front. **3**, 200113 (2024).
[10]A. E. Wilson-Heid, R. J. Griffiths, A. A. Martin, K. S. Holliday, and J. R. Jeffries, "Exploring laser-material interactions of zirconium carbide under additive manufacturing conditions," Ceram. Int. **50**, 23275–23283 (2024).
[11]Z. Liu, C. Ma, Z. Chang, P. Yan, and F. Li, "Advances in crack formation mechanism and inhibition strategy for ceramic additive manufacturing," J. Eur. Ceram. Soc. **43**, 5078–5098 (2023).
[12]Y. Huang, D. Wu, X. Yu, G. Ma, J. Han, H. Wang, and F. Niu, "Cracking mechanism in laser directed energy deposition of melt growth alumina/aluminum titanate ceramics," J. Am. Ceram. Soc. **106**, 4358–4370 (2023).
[13]Z. Chen, C. Liu, J. Li, J. Zhu, Y. Liu, C. Lao, J. Feng, M. Jiang, C. Liu, P. Wang, and Y. Li, "Mechanical properties and microstructures of 3D printed bulk cordierite parts," Ceram. Int. **45**, 19257–19267 (2019).
[14]Y. Zheng, K. Zhang, T. T. Liu, W. H. Liao, C. D. Zhang, and H. Shao, "Cracks of alumina ceramics by selective laser melting," Ceram. Int. **45**, 175–184 (2019).
[15]Z. Liu, C. Ma, Z. Chang, P. Zhao, Y. Zhang, Q. Wu, and F. Li, "Formation mechanism and quantitative analysis of pores in $Al2O_3$–ZrO_2 ceramic different structures by laser additive manufacturing," Ceram. Int. **49**, 16099–16109 (2023).
[16]J. Zhang, J.-M. Wu, H. Liu, W. Zheng, C.-S. Ye, S.-F. Wen, C.-Z. Yan, and Y.-S. Shi, "Microstructure and properties of silica-based ceramic cores by laser powder bed fusion combined with vacuum infiltration," J. Mater. Sci. Technol. **157**, 71–79 (2023).
[17]T. S. Munonde and M. C. Raphulu, "Review on titanium dioxide nanostructured electrode materials for high-performance lithium batteries," J. Energy Storage **78**, 110064 (2024).
[18]K. Liu, M. Cao, A. Fujishima, and L. Jiang, "Bio-inspired titanium dioxide materials with special wettability and their applications," Chem. Rev. **114**, 10044–10094 (2014).
[19]S. Mukherjee and A. K. Mukhopadhyay, "2-Advanced processing and characterization of ceramic-based multilayers," in *Advanced Ceramic Coatings for Energy Applications*, edited by R. K. Gupta, A. Motallebzadeh, S. Kakooei, T. A. Nguyen, and A. Behera (Elsevier, New York, 2024), pp. 17–37.
[20]L. Treccani, "Introduction to ceramic materials," in *Surface-Functionalized Ceramics* (John Wiley & Sons, Ltd, New York, 2023), pp. 1–46.
[21]A. Ullah, H. Wu, A. Ur Rehman, Y. Zhu, T. Liu, and K. Zhang, "Influence of laser parameters and Ti content on the surface morphology of L-PBF fabricated titania," Rapid Prototype J. **27**, 71–80 (2021).
[22]A. Ullah, A. Ur Rehman, M. U. Salamci, F. Pıtır, and T. Liu, "The influence of laser power and scanning speed on the microstructure and surface morphology of Cu_2O parts in SLM," Rapid Prototype J. **28**, 1796–1807 (2022).
[23]A. Ur Rehman, A. Ullah, T. Liu, R. Ur Rehman, and M. U. Salamci, "Additive manufacturing of Al_2O_3 ceramics with MgO/SiC contents by laser powder bed fusion process," Front. Chem. **11**, 1034473 (2023).
[24]K. Zhang, S. Li, T. Liu, Z. Xiong, Z. Zhu, Y. Zhang, A. Ullah, and W. Liao, "Broadening the microstructure regime of Al_2O_3–ZrO_2 hypereutectic ceramic fabricated via laser powder bed fusion," Smart Mater. Manuf. **2**, 100048 (2024).
[25]Y. Zhang, K. Zhang, D. Chen, T. Liu, Z. Xiong, S. Li, F. Li, and Z. Zhu, "Morphology and formation mechanism of cracks in Al_2O_3–ZrO_2 eutectic ceramics fabricated via laser powder bed fusion," J. Am. Ceram. Soc. **107**, 2128–2142 (2024).
[26]Z. Xiong, K. Zhang, T. Liu, Z. Zhu, H. Wei, Z. Zou, and W. Liao, "Role of scanning speed on the microstructure and mechanical properties of additively manufactured Al_2O_3–ZrO_2," J. Am. Ceram. Soc. **106**, 7760–7775 (2023).
[27]T. L. Bergman, *Fundamentals of Heat and Mass Transfer*, 6th ed. (Wiley, Hoboken, 2011).
[28]L. Moniz, Q. Chen, G. Guillemot, M. Bellet, C.-A. Gandin, C. Colin, J.-D. Bartout, and M.-H. Berger, "Additive manufacturing of an oxide ceramic by laser beam melting—Comparison between finite element simulation and experimental results," J. Mater. Process. Technol. **270**, 106–117 (2019).
[29]T. Mukherjee and T. Debroy, "Mitigation of lack of fusion defects in powder bed fusion additive manufacturing," J. Manuf. Process. **36**, 442–449 (2018).
[30]T. P. Moran, D. H. Warner, A. Soltani-Tehrani, N. Shamsaei, and N. Phan, "Spatial inhomogeneity of build defects across the build plate in laser powder bed fusion," Addit. Manuf. **47**, 102333 (2021).
[31]H. Gong, K. Rafi, H. Gu, T. Starr, and B. Stucker, "Analysis of defect generation in Ti–6Al–4V parts made using powder bed fusion additive manufacturing processes," Addit. Manuf. **1–4**, 87–98 (2014).
[32]Kh. Moeinfar, F. Khodabakhshi, S. F. Kashani-bozorg, M. Mohammadi, and A. P. Gerlich, "A review on metallurgical aspects of laser additive manufacturing (LAM): Stainless steels, nickel superalloys, and titanium alloys," J. Mater. Res. Technol. **16**, 1029–1068 (2022).
[33]L. M. Hogan, "Crystals, dendritic solidification of," in *Encyclopedia of Materials: Science and Technology*, edited by K. H. J. Buschow, R. W. Cahn, M. C. Flemings, B. Ilschner, E. J. Kramer, S. Mahajan and P. Veyssière (Elsevier, Oxford, 2001), pp. 1913–1918.
[34]R. Acharya, J. Sharon, and A. Staroselsky, "Prediction of microstructure in laser powder bed fusion process," Acta Mater. **124**, 360–371 (2017).
[35]B. Lu, Y. Li, H. Wang, Y. Wang, W. Yu, Z. Wang, and G. Xu, "Effects of cooling rates on the solidification behavior, microstructural evolution and mechanical properties of Al–Zn–Mg–Cu alloys," J. Mater. Res. Technol. **22**, 2532–2548 (2023).
[36]J. Wang, R. Zhu, Y. Liu, and L. Zhang, "Understanding melt pool characteristics in laser powder bed fusion: An overview of single- and multi-track melt pools for process optimization," Adv. Powder Mater. **2**, 100137 (2023).
[37]S. N. Tedman-Jones, S. D. McDonald, M. J. Bermingham, D. H. StJohn, and M. S. Dargusch, "A new approach to nuclei identification and grain refinement in titanium alloys," J. Alloys Compd. **794**, 268–284 (2019).
[38]L. Kang and C. Yang, "A review on high-strength titanium alloys: Microstructure, strengthening, and properties," Adv. Eng. Mater. **21**, 1801359 (2019).
[39]Z. Xiong, K. Zhang, Z. Zhu, T. Liu, Y. Zhang, S. Li, and W. Liao, "Effect of laser focus shift on the forming quality, microstructure and mechanical properties of additively manufactured Al_2O_3–ZrO_2 eutectic ceramics," Ceram. Int. **49**, 35948–35962 (2023).
[40]M. Zheng, L. Wei, J. Chen, Q. Zhang, G. Zhang, X. Lin, and W. Huang, "On the role of energy input in the surface morphology and microstructure during selective laser melting of Inconel 718 alloy," J. Mater. Res. Technol. **11**, 392–403 (2021).